Feature-based multibody rigid registration of CT and ultrasound images of lumbar spine

Abtin Rasoulian and Purang Abolmaesumi[a)]
Electrical and Computer Engineering, University of British Columbia, 2332 Main Mall, Vancouver, British Columbia V6T 1Z4, Canada

Parvin Mousavi
School of Computing, Queen's University, 25 Union Street, Goodwin Hall, Kingston, Ontario K7L 3N6, Canada

(Received 31 October 2011; revised 6 March 2012; accepted for publication 18 April 2012; published 15 May 2012)

Purpose: Fusion of intraprocedure ultrasound and preprocedure CT data is proposed for guidance in percutaneous spinal injections, a common procedure for pain management. CT scan of the lumbar spine is usually collected in a supine position, whereas spinal injections are performed in prone or sitting positions. This leads to a difference in the spine curvature between CT and ultrasound images; as such, a single-body rigid registration approach cannot be used for the whole lumbar vertebrae.
Methods: To compensate for the difference in the spinal curvature between the two imaging modalities, a multibody rigid registration algorithm is presented. The approach utilizes a point-based registration technique based on the unscented Kalman filter (UKF), taking as input segmented vertebrae surfaces in both CT and ultrasound data. Ultrasound images are automatically segmented using a dynamic programming method, while the CT images are semiautomatically segmented using thresholding. The registration approach is designed to simultaneously align individual groups of points segmented from each vertebra in the two imaging modalities. A biomechanical model is developed to constrain the vertebrae transformation parameters during the registration and to ensure convergence.
Results: The proposed methodology is evaluated on human spine phantoms and a sheep cadaver. Registrations on phantom data have a mean target registration error (TRE) of 1.99 mm in the region of interest and converged in 87% of cases. Registrations on sheep cadaver have a mean target registration error of 2.2 mm and converged in 82% of cases.
Conclusions: The proposed technique can robustly and simultaneously register several vertebrae extracted from CT images to the ultrasound volumes. The registration error below 2.2 mm is sufficient for most spinal injections. © *2012 American Association of Physicists in Medicine*. [http://dx.doi.org/10.1118/1.4711753]

Key words: ultrasound, CT, multibody registration, spinal injections

I. INTRODUCTION

Lower back pain is one of the most commonly reported forms of discomfort in the average workforce, leading to decreased quality of life, time away from work, and dramatic decline on performance. First-line therapies focus on conservative nonoperative care through custom physical therapy programs and medication. However, these interventions only lead to short-term reduction of pain, with less than 20% sustained pain relief in long term.[1] When oral medication fails, some form of spinal injection, such as steroid injection, is considered. These injections are mostly performed by inserting a fine needle into the facet joint between two vertebrae (Fig. 1). This is a challenging procedure due to the narrow space between facets [between 2 and 4 mm (Ref. 2)] and proximity to nerve tissue. The procedure is normally guided by fluoroscopic imaging to direct the needle to the targeted injection site, resulting in significant increase in its accuracy.[3] Although the injection is safe and more accurate with this approach, there are several disadvantages to using two-dimensional (2D) fluoroscopic guidance. The most notable is exposure to ionizing radiation by the clinician and the patient. Other limitations include insufficient information in 2D projections for accurate presentation of needle trajectory and depth of insertion.

In search of a more accessible, portable, and nonionizing imaging alternative, there has been a resurgence in the application of ultrasound imaging for guiding percutaneous spinal injections.[4] Current evidence suggests that ultrasound-guided facet injections have a similar success rate to those of conventional procedures.[5] However, despite their advantages for both patients and clinicians, ultrasound-guided procedures have yet to become the standard-of-care for pain management. The main obstacles to this are the poor quality depiction of anatomical features, poor visibility of the needle in ultrasound images, as well as the difficulty in interpreting images by novice ultrasound users including many anesthesiologists.

To improve guidance with ultrasound imaging, augmenting ultrasound images with preprocedure data such as CT is suggested.[6–12] Although significant advancements have been

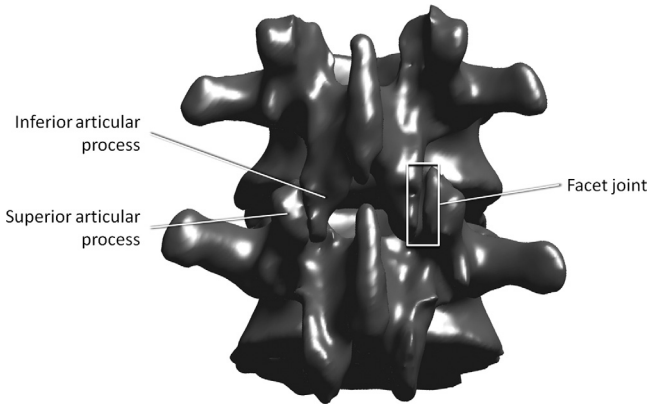

FIG. 1. Facet joints are between the superior articular process of one vertebra and the inferior articular process of the vertebra directly above it. There are two facet joints between each two vertebrae levels.

made for registration of CT and ultrasound images in the case of femure and pelvis for orthopedic surgery applications [see, e.g., Refs. (13–15) among others], automatic registration of ultrasound and CT data of the spine has proved to be a challenging task. Several solutions to this registration problem[16–19] assume a single rigid body registration between preprocedure and intraprocedure data. While the vertebrae do not deform, such assumption does not hold for the majority of spinal needle injection procedures including facet joint injections: CT scan of the lumbar spine is usually collected in a supine position, whereas spinal facet joint injections are performed in prone or sitting positions. This leads to a difference in the spine curvature, i.e., a difference in the relative position of the vertebrae between CT and ultrasound images; as such, a single-body rigid registration approach cannot be used for the whole lumbar vertebrae. Additionally, due to rigid motion of each vertebra, other transformations such as affine and deformable are not applicable. Another difficulty is that the vertebrae cannot be easily distinguished and labeled in the ultrasound images; therefore, registration of each vertebra extracted from the CT images to the corresponding one in the ultrasound images is challenging, even with a good initialization. To address these shortcomings, multibody registration techniques can be used.[20]

Here, we propose a feature-based method for multibody rigid registration of ultrasound and CT data of the lumbar spine. The registration is constrained using a biomechanical model we develop. The prerequisite for such registration is the segmentation of both ultrasound and CT data. Segmentation of CT images can be performed preoperatively. Ultrasound images, on the other hand, have to be segmented intraoperatively. We use an automatic and real-time segmentation technique to extract the surface of the vertebrae from ultrasound data. We also use a point-based registration method involving the unscented Kalman filter (UKF),[21,22] which we previously demonstrated to significantly outperform the popular iterative closest point (ICP) registration approach.[23] Specifically, we take advantage of the robustness of the UKF approach to the existence of outliers in the data sets, which would inevitably be the case for any automatic ultrasound image segmentation. We improve the registration accuracy by developing a technique which sequentially removes outliers during the registration. We integrate our developed biomechanical model in the multibody UKF-based registration approach, presented by Moghari and Abolmaesumi,[22] to constrain the space of solutions for the registration problem. Specifically, the following contributions are made:

(1) Integration of a biomechanical model in the multibody UKF-based registration
(2) Addition of a dynamic outlier removal technique within the registration approach

A biomechanical model was used previously by our research team for the intensity-based registration of a group of vertebrae in ultrasound and CT images,[8] where an energy term, that is linearly dependent on the relative transformations of adjacent vertebrae, is added to the cost function. On the other hand, the biomechanical model used in the proposed feature-based registration method simulates the disk between vertebrae by a spring model. This is slightly more sophisticated than our previous approach, but clearly less accurate than other computationally more intensive techniques such as FEM. The reason for selecting the spring model, as the biomechanical model, is twofold: First, it easily fits into the UKF-based registration approach as will be explained later. Second, it provides an acceptable compromise between model accuracy and computational complexity.

We also introduce a novel outlier removal method that dynamically detects and removes the outliers during the registration. This is generally required in registration problems involving ultrasound images due to many false positives in segmentation of bone surfaces from ultrasound data.

We validate the proposed biomechanically constrained feature-based registration method on data collected from human phantom and sheep cadaver.

II. MATERIALS AND METHODS

A flowchart demonstrating the overall segmentation and registration work flow is shown in Fig. 2. As seen in this figure, the registration method takes as input segmented vertebrae surfaces from both CT and ultrasound data. Tracked 2D ultrasound images are automatically segmented using a dynamic programming method, and the bone surface is reconstructed using the tracking information. The CT images are semiautomatically segmented and labeled. These two point sets are then registered using the biomechanically constrained multibody registration algorithm.

The details of the segmentation, UKF-based registration, and the multibody registration algorithms including the biomechanical model are described below. Throughout the paper, we use the following notations:

- N_v: Number of point sets (vertebrae)
- $\mathbf{U}^j$: The jth moving point set (extracted from jth vertebra in CT images)
- u_i^j: ith moving point belong to $\mathbf{U}^j$

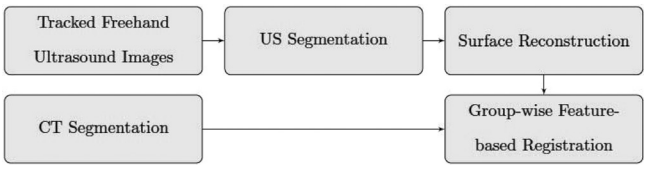

FIG. 2. The workflow of the proposed methodology. Ultrasound images are segmented to identify vertebrae surfaces. By using the tracking information, a 3D representation of vertebrae surface is generated. Using segmented CT volume, a point-based registration method is applied to register the two point sets.

- $\mathbf{Y}$: The fixed point set (extracted from ultrasound images)
- y_i^j: The corresponding point to u_i^j, selected from fixed point set, $\mathbf{Y}$
- Σ_i^j: Covariance matrix of an isotropic noise associated with corresponding points u_i^j and y_i^j
- R^j, t^j: Rotation and translation associated with the jth moving point set
- N_s: Number of springs

II.A. A CT image segmentation

We apply a semiautomatic segmentation technique to identify the surface of vertebrae from CT images. First, the CT volume is cropped manually to separate vertebrae from each other. Then, each vertebra is segmented semiautomatically using thresholding in the publicly available software, ITK-SNAP. Possible mis-segmentations are corrected manually. This approach is applied to both phantom data and sheep cadaver. Similar to Winter *et al.*,[12] only parts of the vertebra surface facing the ultrasound transducer are used in the registration process. Since the ultrasound transducer is normally placed on patients' back in sagittal or transverse direction during spine interventions, the ultrasound beam has a posterior–anterior direction, and hence, only the posterior parts of the vertebrae (i.e., spinouse process, laminae, and transverse processes) are visible. Confining the CT points to those normally visible by the ultrasound transducer will improve the registration convergence. Resulted point sets constitute $\mathbf{U}^j$, the moving point sets. Given that this process is performed before the procedure, it is not a time critical component of the registration task.

II.B. Ultrasound segmentation

The surfaces of vertebrae are segmented from ultrasound images using an algorithm initially proposed by Foroughi *et al.*[24] In that algorithm, the ultrasound images are first smoothed to minimize the effect of speckle. Next, the appearance of the bone surface, referred to as bone probability, is enhanced for each pixel in the image using its intensity value and shadow information extracted from neighboring pixels. Finally, dynamic programming is used to segment the bone surface by minimizing a cost function based on the bone probability together with the continuity and smoothness of the segmented surface. The original algorithm[24] uses a Gaussian filter as the smoothing function. Here, this function is replaced by filtering the image using the Sticks filter followed by the anisotropic diffusion[25] [see Figs. 3(b) and 3(c)]. Sticks filter is shown to be a very powerful tool to enhance the boundaries in ultrasound images.[26] For each pixel in the image, the algorithm finds the line with length N that is centered on the pixel and has the maximum gray-level summation. The algorithm assigns this summation to the pixel. We performed Sticks filter with $N = 15$. Czerwinski *et al.* showed that combination of the Sticks filter and the anisotropic diffusion is superior to Gaussian since it preserves the edges while removing the speckles.[25] Next, we use the approach proposed by Foroughi *et al.*[24] to calculate the bone probability for each pixel in the ultrasound image [Fig. 3(d)]. Finally, dynamic programming is used to segment the bone surface. The segmented image is depicted in Fig. 3(e) [compared to the gold standard segmentation shown in Fig. 3(a)]. The ultrasound transducer is tracked using an Optotrak Certus System (Northern Digital, Inc., Waterloo, Ontario, Canada) and is calibrated using an N-wire US phantom.[27] The calibration has an average point reconstruction error[28] of 0.66 mm. The tracking information together with ultrasound probe calibration provides the transformation from all 2D tracked ultrasound images to the physical space. The union of all transformed sets of segmented points from 2D ultrasound frames constitutes $\mathbf{Y}$, the fixed point set. A segmented ultrasound image is shown in Fig. 3(e).

II.C. Biomechanical model

A biomechanical model is developed to constrain the displacement of the vertebrae relative to one another and to eliminate the possibility of converging to an unrealistic curvature of the spine during registration of CT and ultrasound data. We build our model by defining groups of springs between each two vertebrae to resemble the intervertebral disc [see Fig. 4(a)]. Details are shown in Fig. 4. To position the springs, the center of the mass of each vertebra is calculated from the CT volume data. Assume that c is the center of a line connecting these two points [Fig. 4(b)]; two parallel 2D grids are placed orthogonal to this line where their center is aligned on the line. Each grid has a distance of $d/2$ from the center c. The grids, each with size r, are divided into n_g cells in each direction. Large n_g will lead to more accurate simulation of discs and consequently a more accurate model, but slower registration. Springs are placed orthogonal to the grids in between each two corresponding grid cells. Parameters d and r are found based on realistic measurement of vertebrae dimensions.[29] The upper lumbar vertebra has a width in the range of 30–50 mm. The intervertebral disc has a height in the range of 8–16 mm. Based on these values, and the measurements in our data, we selected the parameters r and d to be $r = 40$ mm and $d = 10$ mm. We keep these values constant for all intervertebral spaces.

Relative transformations of vertebrae result in changes to the springs' lengths [see Fig. 4(c)]. The springs obey Hooke's law which states that the force with which the spring pushes back is linearly proportional to the distance from its equilibrium length. Therefore, the biomechanical model regularization term can be written as

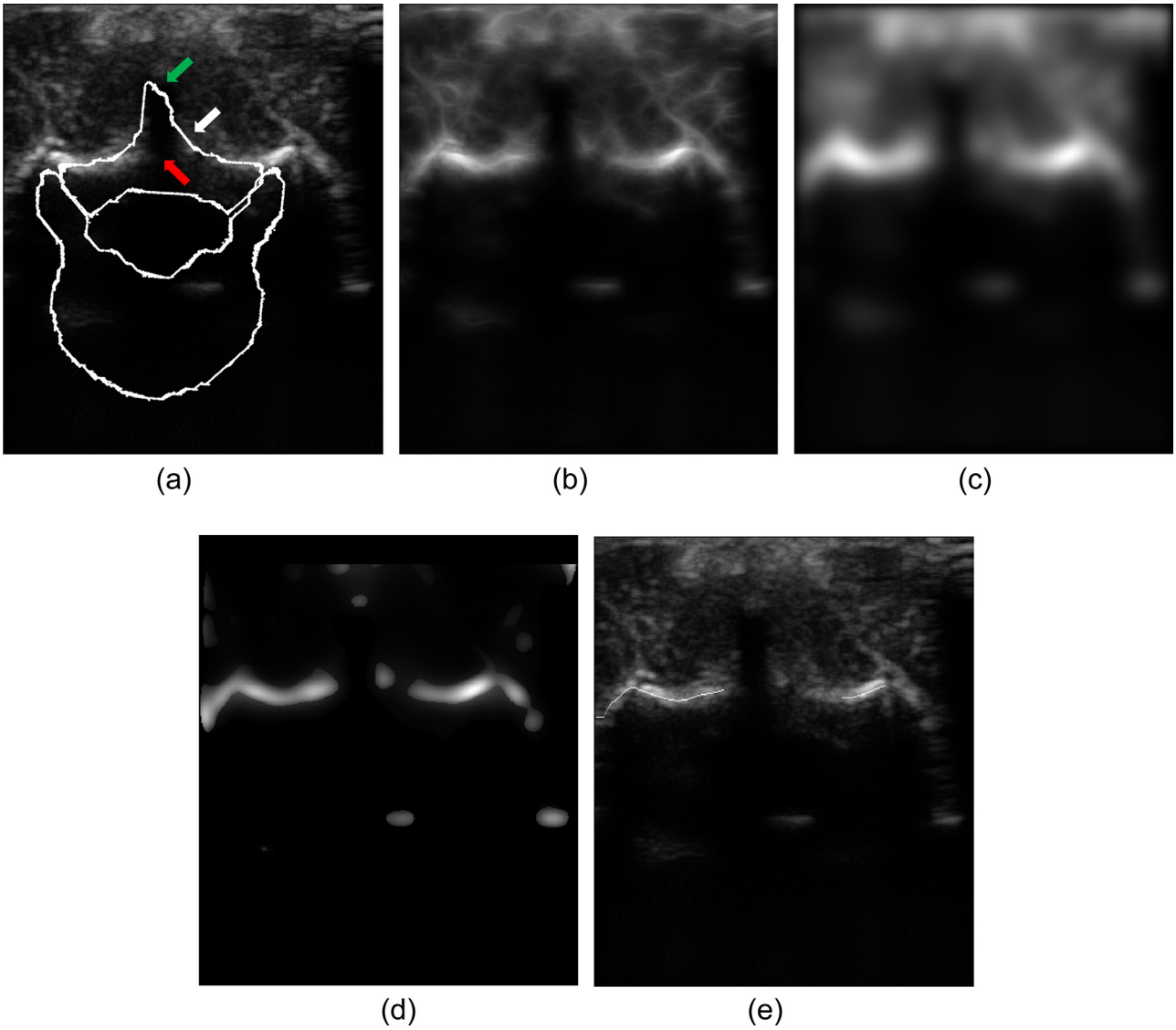

FIG. 3. Intermediate steps in the segmentation of an ultrasound frame captured from the sheep cadaver. (a) Gold standard segmentation of the ultrasound image captured from sheep cadaver. The image is taken in transverse direction with spinous process (top arrow) centered. The discontinuity (bottom arrow) is to be expected since the parts of the surface [i.e., laminae (middle arrow) in this frame] which are not perpendicular to the ultrasound beam cannot be visualized well in ultrasound images. (b) Sticks filter followed by (c) anisotropic diffusion is used to smooth the image; (d) the bone probability is extracted for each pixel in the image using its intensity value and shadow information; (e) the final segmentation overlaid on the ultrasound image.

$$\mathbf{G} = \frac{1}{N_s}\sum_{k=1}^{N_s} |\Delta s_k|, \tag{1}$$

where $|\Delta s_k|$ stands for absolute change in length of kth spring. Since the relative motion of adjacent vertebrae is relatively small (i.e., less than 5 mm, 10° between ultrasound and CT images), we found the linear model to be sufficient for our application. This regularization is incorporated in the registration cost function as shown in Sec. II.D.

II.D. Biomechanically constrained multibody rigid UKF-based registration

The pair-wise UKF-based surface registration originally proposed by Moghari and Abolmaesumi[21] is an iterative registration method that minimizes mean squared distance error between two point sets, u_i and y_i, as follows:

$$\mathbf{E}_{(R,t)} = \sum_{i=1}^{l} (y_i - Ru_i - t)^T (\Sigma_i)^{-1} (y_i - Ru_i - t). \tag{2}$$

Initially, l, the number of points involved in the registration, is small and has to be greater than four. In each iteration of the registration, l is incremented by one and the registration parameters (i.e., translation and rotation), which are considered as the state variables, are estimated by minimizing the L2 norm of the distances between corresponding points in moving and fixed point sets. We refer the reader to the work presented by Moghari and Abolmaesumi[21] for a detailed discussion on the superior performance of the UKF-based registration over ICP in terms of capture range and robustness to outliers. In summary, both algorithms work in a similar fashion with two major differences: First, the UKF-based registration

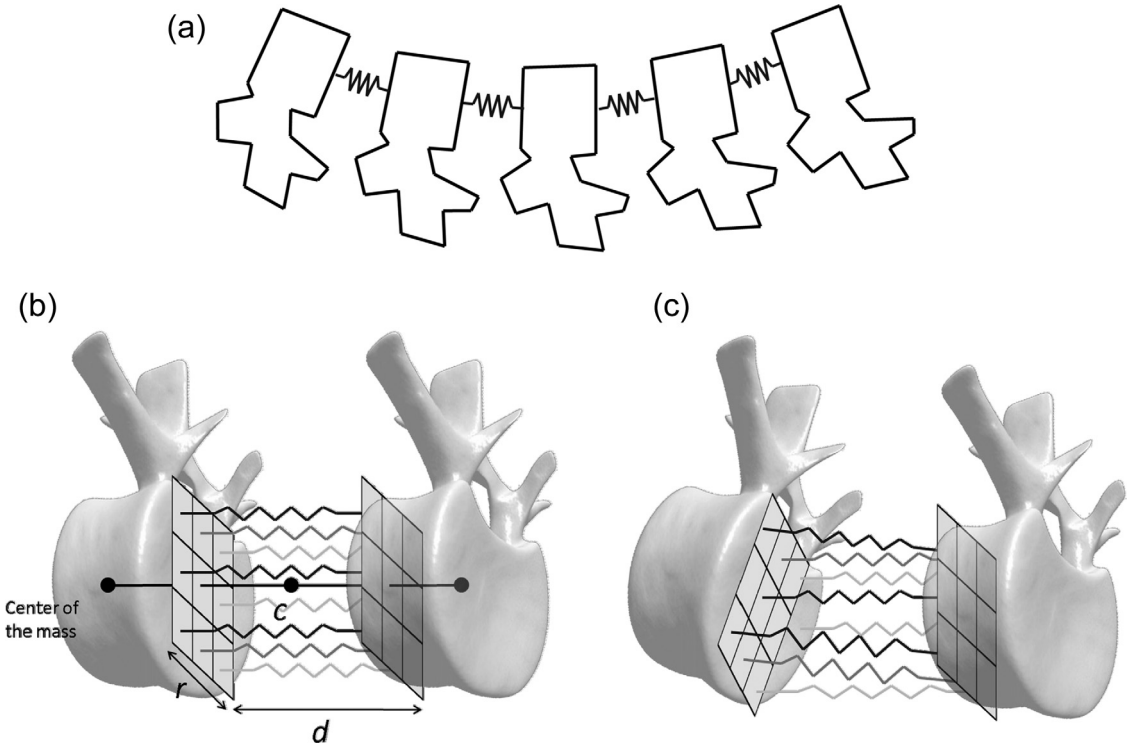

FIG. 4. (a) Groups of springs are defined between each two vertebrae to resemble the intervertebral disc. (b) Spring model: Two grids are placed between each two vertebrae perpendicular to the line connecting their center of mass. Springs are positioned between each corresponding cells of these two grids. (c) Deformed model; The springs' original lengths are not preserved.

incrementally processes the points in the data sets, which leads to improved computation time. Second, the UKF-based registration uses the variance of noise distribution in the point sets and the estimated variance of the registration transformation parameters to deal with outliers. The latter also significantly improves the capture range of the algorithm over the ICP that only uses the closest point distances to optimize the registration parameters.

Moghari and Abolmaesumi later on extended their registration technique to multibody registration of multiple point sets,[22] with the following cost function:

$$\mathbf{E}_{(R,t)} = \sum_{j=1}^{N_v} \sum_{i=1}^{l} (y_i^j - R^j u_i^j - t^j)^T (\Sigma_i^j)^{-1} (y_i^j - R^j u_i^j - t^j). \quad (3)$$

Here, we extend the multibody registration method to include a biomechanical model to constrain the general spine motion during registration. The overall cost function is a weighted summation of the matching cost function, $\mathbf{E}$, and the biomechanical model regularization term, $\mathbf{G}$

$$\mathbf{C} = \alpha \mathbf{E} + (1 - \alpha)\mathbf{G}, \quad (4)$$

where α is the trade-off variable between two parts. The registration approach itself (i.e., the UKF-based registration to minimize the corresponding point distances) is not modified; as a result the convergence property is preserved if the initial values for the registration parameters are within the capture range for the correct solution. $\alpha = 1$ removes the biomechanical model, whereas α close to 0 preserves the spine initial curvature and the registration acts similar to a rigid one. The final cost function can be written as

$$\mathbf{C} = \frac{\alpha}{N_v l} \sum_{j=1}^{N_v} \sum_{i=1}^{l} (y_i^j - R^j u_i^j - t^j)^T (\Sigma_i^j)^{-1} (y_i^j - R^j u_i^j - t^j) + \frac{(1-\alpha)}{N_s} \sum_{k=1}^{N_s} |\Delta s_k|. \quad (5)$$

Note that both parts of the cost function are normalized with respect to their input size ($N_v l$ and N_s). The multibody rigid algorithm steps are outlined below.

Require: labeled extracted surface of the bone from the CT images, U^j, and the bone surface from the ultrasound images, Y. initialize each $u_{1:l}^j$ with a subset of U^j.
repeat
increment l by appending a random point from each set U^j to subsets $u_{1:l}^j$.
for $j = 1$ to N_v **do**
$y_{1:l}^j \leftarrow$ the nearest points from Y to $u_{1:l}^j$.
end for
minimize cost function in Eq. (5) (including minimization of $|\Delta s_k|$ and the distances between y_i^j and u_i^j); use UKF to estimate R^j and t^j.
update distances between corresponding points in U^j and Y.
remove outliers
until converge

II.E. Outlier removal

Automatic segmentation of ultrasound images usually produces many outliers. By including the outliers in the registration, the process may converge to a local minimum.

Barratt *et al.*[15] suggest an approach to improve registration by removing outliers. In their approach, a conventional rigid-body registration is performed. Next, outliers are automatically removed by transforming the ultrasound points using the updated registration transformation and removing 10% of the points that are farthest from the CT bone surface. Once outliers have been removed, a second rigid-body registration is performed using the remaining ultrasound points. We found this approach not to be robust enough to handle inputs with high number of outliers. We modified this algorithm to sequentially remove outliers during each iteration of registration as described below.

After each iteration of the registration, outliers are automatically detected and removed based on a weighted average of their distances from the fixed point set during all previous iterations. Assume $d_{i,t}$ to be the ith ultrasound point's distance to its nearest CT point, that is, $d_{i,t} = \|y_i - Ru_i - t|$, at iteration t. A weighted average of distances during the registration is taken using

$$\tilde{d}_i = \frac{\sum_{t=1}^{l} t \log(d_{i,t})}{l(l+1)}, \tag{6}$$

where t assigns higher weight to the current iteration and less to all previous iterations. In our initial experiments, the logarithmic distance outperformed linear distance. Distances have a very high dynamic range (0–15 mm) due to the outliers in ultrasound images. Our interpretation is that by using the logarithm of distances, the effect of outliers is reduced. In each iteration, the following condition will be used to remove outliers:

$$\begin{aligned} &\text{if } \tilde{d}_i > \log(E[\tilde{d}_i] + d_{thr}) \\ &\text{then remove point,} \end{aligned} \tag{7}$$

where $E[\tilde{d}_i]$ is the average distance of all $\tilde{d}_i$. Addition of $E[\tilde{d}_i]$ is needed since at the beginning all points have large distances to their corresponding points and should not be removed as outlier. In our experiments, we set d_{thr} to be 3 mm. There are two main reasons behind selecting 3 mm as the threshold. First, the ultrasound segmentation has root mean square (RMS) error of 1 mm (Ref. 24) which suggests removing points with distance above $3 \times \sigma = 3 \times 1$ mm as outliers (confidence interval of 99%). Second, this threshold value is used in other similar works on CT to ultrasound registration.[21]

III. EXPERIMENTAL EVALUATION

III.A. Data acquisition and reference registration

Our proposed registration approach is evaluated with two different types of data: tissue mimicking phantoms created from human spine and a sheep cadaver. The phantoms were created by segmenting the surface points of L1–L5 vertebrae from the CT data of five patients and generating a 3D physical model of the lumbar vertebrae using a Dimension SST 3D printer (Stratasys, Inc., Eden Prairie, MN). The CT data were collected at Kingston General Hospital where the patients provided informed consent to participate in the research. The natural curvature of the spine is maintained between the patient CT and the printed model. The printed vertebrae were mounted in a plastic container, which was filled with an agar–gelatin mixture. CT-visible fiducial markers were then placed at various locations on the outside surface of the phantom container, followed by a CT scan of the entire phantom with 0.46 mm × 0.46 mm × 0.625 mm resolution.

The sheep cadaver was chosen as it was found to sufficiently resemble the human spine, particularly in the thoracic and lumbar area.[30] The sheep cadaver used for data collection included five lumbar vertebrae (L1–L5) and had undergone rigamortis and cooling for storage. The cadaver was placed in a plastic container. Similar to phantoms, fiducial markers were attached to the container box, and CT data were acquired at the resolution of 0.7 mm × 0.7 mm × 0.625 mm.

Experiments were also performed on a patient-based curved phantom, with three vertebrae (L2–L4) to assess the robustness of the algorithm to realistic deformation of the spine curvature. To this end, ultrasound and CT data were collected twice from a patient-based phantom: once with the model retaining the natural curvature of the spine and once with introducing an approximately 4° curvature between the vertebrae, along the transverse axis. CT-visible fiducials were placed on each vertebra and were manually segmented in all CT images of phantoms and the sheep cadaver.

Prior to collecting a freehand ultrasound scan of the phantoms, the locations of the fiducial markers were determined using an optically tracked calibrated stylus and a Certus camera system (Northern Digital Inc., Waterloo, Ontario, Canada). Then, the transformation from the CT coordinates to the ultrasound image coordinates was computed by registering the fiducial markers using Horn's method.[31] Two-dimensional B-mode ultrasound images of the phantoms and cadaver were then acquired using a Sonix RP ultrasound machine (Ultrasonix Medical Corp., Richmond, Canada) with a linear-array transducer, operating at 6.6 MHz with a depth setting of 5.5 cm. The number of ultrasound frames acquired from each phantom and the sheep cadaver ranged from 190 to 245. This, for all data, results in a spatial resolution of about 0.2 mm × 0.2 mm × 1 mm. The ultrasound transducer was calibrated using an N-wire phantom[27] and tracked by the Certus system. Figure 5 shows the acquisition setup for the sheep cadaver.

III.B. Evaluation

Two types of registration are performed on both phantom and sheep data: rigid and multibody registration.

III.B.1. Rigid registration

Rigid registration is performed on all subjects each including five vertebrae. This experiment is only performed to establish the applicability of the outlier removal and superiority of the UKF-based registration to ICP in terms of accuracy. The ultrasound data, which is registered to CT using the gold standard (e.g., the fiducial markers) and

FIG. 5. Acquisition setup for the sheep cadaver. White arrow shows the fiducial markers attached to the container. Red arrow shows the spatial localizer attached to the ultrasound transducer.

includes all five vertebra (L1–L5), are perturbed by a transformation with translation and rotation parameters drawn randomly within ± 10 mm and $\pm 10°$. The transformation is centered at center of the middle vertebra, L3. The target registration error (TRE) is calculated based on the bounding box which is placed around all five vertebrae together. This is referred to as TRE_b hereafter. The initial misalignment generates initial TRE_b ranging from 0 to 20 mm. A registration is considered successful if the final TRE_b is less than 3 mm. For facet joint injections, a target accuracy of 5 mm has been reported to be sufficient.[32] Our proposed 3 mm accuracy requirement would lead to a 95% confidence interval of 6 mm for predicting the needle tip location. The registration is performed 100 times, with different initial misalignments, on each phantom and the sheep cadaver.

We evaluate different outlier removal techniques using the rigid registration algorithm. Here, we report the results on phantom data only (similar results are observed for the cadaver).

III.B.2. Multibody rigid registration

Multibody rigid registration is performed on five lumbar spine (L1–L5). To simulate the deformation in spine curvature, in each trial, the subvolume containing each vertebra in CT, where voxels belonging to other vertebrae are removed, is perturbed individually using translation and rotation parameters drawn randomly within ± 5 mm and $\pm 5°$, using a uniform distribution. Another global perturbation was also applied to the CT data to simulate the displacement between preprocedure and intraprocedure data. This global transformation includes translation and rotation parameters drawn randomly within ± 7 mm and $\pm 7°$. The local transformations are centered at each vertebra, whereas the global transformation is centered at the center of the middle vertebra, L3. The first error is calculated based on the bounding box of each vertebra and is also referred to as TRE_b. This error represents the worse case scenario since the facet joint, the injection target in this research, is close to the middle of the bounding box and will have lower errors compared to the bounding box. The initial misalignment generates initial TRE_b ranging from 0 to 20 mm for all except the middle vertebra (L3). For L3, the initial misalignments are in the range of 0–15 mm, as the global transformation is centered at this vertebra. The overall TRE_b of the registration is the average of TRE_b of all vertebrae. In our study, we selected the acceptable registration TRE_b to be less than 3 mm as suggested by Gill *et al.*;[8] this is deemed as an acceptable accuracy for facet joint interventions.[18] Additional to TRE_b, another error is calculated to reveal the accuracy of registration around facet joints. To this end, a point is selected on inferior articular processes of each vertebra. For each selected point, all the points in the CT segmented surface with a radius of 7 mm are extracted. Facet joints may have a width and height between 10 and 18 mm,[33] therefore the radius of 7 mm guarantee to cover enough number of points on facet joints. An example of extracted surface around facet joint is depicted in Fig. 6. Initial selected points are shown in red color. The extracted surface is highlighted by white color. An error is defined as the distance between these points transformed by the gold standard and our registration transformations. RMS of these distances is computed and is referred to as TRE_f hereafter. Normal facet joint space may have width of 2–4 mm.[2] In our study, we selected the acceptable registration TRE_f to be less than 3 mm.

In case of patient-based curved phantom, experiments are only performed on multibody registration, since the rigid registration is not capable of aligning images captured from spines with different curvature. After each multibody registration, average of distances between corresponding fiducials placed on each vertebra is computed and is reported as TRE.

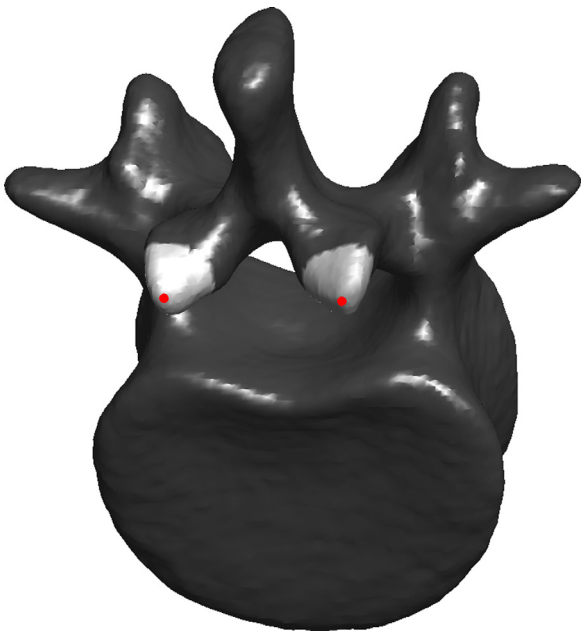

FIG. 6. Extraction of a surface around facet joints. Initial point, which is selected manually, is shown by a red dot. The surfaces around these points are extracted with a radius of 7 mm. Surfaces are highlighted with white color.

Capture range. Another set of registrations are performed to assess the capture range of the multibody registration. Initial misalignment is generated with the same range as before (local translation and rotation within ±5 mm and ±5° and global translation and rotation within ±7 mm and ±7°, respectively). However, this time, parameters are chosen such that the average of initial misalignment (TRE_b) of all vertebrae in each trial falls into four equal intervals from 0–4 to 12–16 mm. The percentage of success (final TRE_b <3 mm) is then computed for each vertebra in each interval.

Multibody rigid registration parameters. Additional to these experiments, effectiveness of the main parameters of the multibody registration algorithm is measured. The result for this part can be found in Sec. IV.E. The multibody rigid registration algorithm includes two main parameters, α and n_g. Parameter α controls the trade-off between registration accuracy and preservation of initial vertebrae curvature, and n_g controls the number of springs defined between each two vertebrae.

The effectiveness of the biomechanical model can be measured using the trade-off parameter α in Eq. (5). To evaluate the relation between algorithm's performance and α, we performed 20 trials, each with different initial misalignment (local translation and rotation within ±5 mm and ±5°, and global translation and rotation within ±7 mm and ±7°, respectively), for each value of $\alpha \in \{\varepsilon, 0.1, 0.2 \ldots 1\}$ on the phantom data. Note that $\alpha = 0$ removes the matching cost in objective function and consequently freeze the moving object. To alleviate this problem, we choose a value close to zero. We selected ε to be 10^{-3}. For all the registrations, the grid size is set to 2×2 $(n_g = 2)$.

The effectiveness of the number of springs between each two adjacent vertebrae is subject of another experiment. To this end, 20 trials (each with different initial misalignment) are performed for each number of grid size ($n_g = 1, 2, 3, 4$) on the phantom data. Here, α is set to 0.1.

IV. RESULTS

IV.A. Ultrasound segmentation

After aligning the ultrasound and CT images using fiducial markers, the accuracy of the ultrasound segmentation is calculated by taking the segmented points' shortest distance to the CT surface. Points with distance more than 3 mm are assumed to be outliers. The results for the originally suggested Gaussian smoothing[24] and our method using Sticks filter and anisotropic diffusion are shown in Table I. The values are the average of 20 random ultrasound frames of phantom data (four frames from each phantom). The results suggest that our proposed approach is more reliable with respect to outliers' generation. Additionally, it generates more number of segmented points. This is important since the performance of the point-based registration algorithm depends on discretization of the data.

TABLE I. Performance of the ultrasound segmentation algorithm using different smoothing functions.

Smoothing function	Segmented points	Mean ± SD	Outliers
Gaussian	489	1.6 ± 0.9	18%
Sticks filter + anisotropic diffusion	1141	1.4 ± 0.5	9%

IV.B. Phantom data registration

IV.B.1. Rigid registration

Rigid registration is performed on five phantoms each including five vertebrae (L1–L5). The registration is performed with and without outlier removal. Both the method proposed by Barratt *et al.*[15] and our approach are used for outlier removal. For comparison purposes, the same experiment is also performed using the standard ICP (without any outlier removal). The registration is performed 100 times on each phantom. Table II shows the final TRE_b for each phantom and success rate for each approach.

The ICP algorithm gets trapped in local minimum in many trials (success rate = 7%). On the other hand, the UKF-based registration is more robust than ICP and converges to better minimum (success rate = 13%). Additionally, excluding outliers improves the registration. The removal approach presented by Barratt *et al.* has higher final TRE_b and is less robust (success rate = 28%) with respect to our proposed approach (success rate = 90%).

IV.B.2. Multibody rigid registration

We perform the validation of multibody registration technique on the phantom data by setting $\alpha = 0.1$ and $n_g = 2$. An example of the registration results is shown in Fig. 7. The registration is performed 100 times.

Table III shows the final error and success rate for each vertebra separately and for the average of them. Registered vertebrae have a mean TRE_b of 2.47 mm with a standard deviation of 1.4 mm and success rate of 88%. All the phantom data have success rates above 90% except the one belonging to patient 2. This is due to its poor registration of L5. Looking closely at the data, we found out that number of

TABLE II. TRE_b for rigid-body registration using ICP, UKF-based method with and without outlier removal for 100 registration trials on each phantom.

Patient	ICP without outlier removal	UKF without outlier removal	UKF with outlier removal (method 1)[a]	UKF with outlier removal (method 2)[b]
1	3.39 ± 0.0	5.55 ± 3.09	4.23 ± 1.43	1.25 ± 1.75
2	28.6 ± 0.2	4.05 ± 2.74	3.24 ± 2.93	3.37 ± 2.77
3	15.1 ± 11.8	4.77 ± 1.04	4.09 ± 0.95	1.97 ± 1.09
4	29.6 ± 0.0	7.79 ± 2.38	5.81 ± 1.75	2.31 ± 2.83
5	4.04 ± 0.0	7.76 ± 3.80	6.53 ± 4.48	2.99 ± 3.93
All	11.2 ± 11.1	6.00 ± 3.14	4.78 ± 2.38	2.38 ± 2.75
Success (%)	7	13	28	90

[a]Outlier removal approach followed by Barratt *et al.* (Ref. 15).
[b]The proposed outlier removal approach.

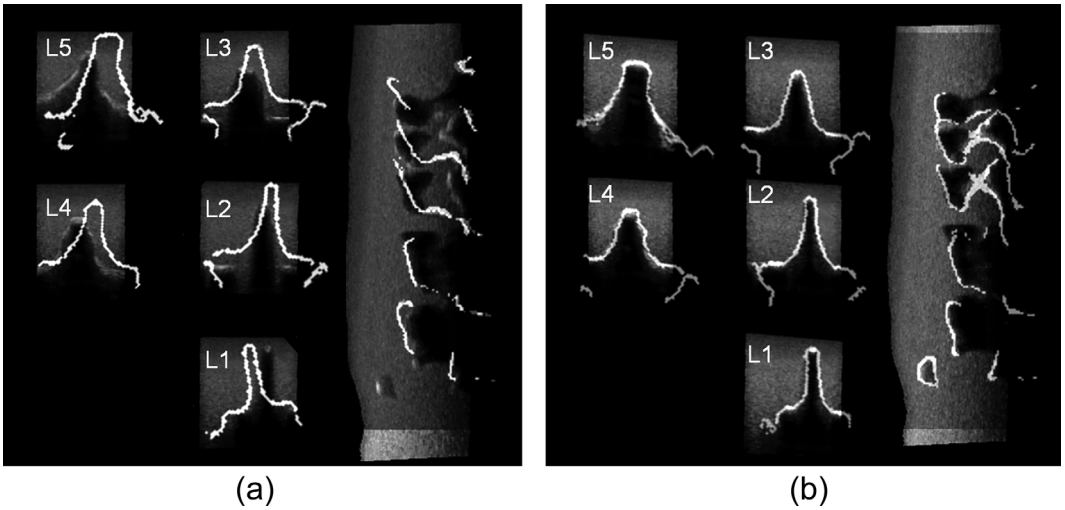

FIG. 7. An example of registration performed on phantom data. (a) The initial alignment of ultrasound and CT points and (b) the final alignment after registration. The first two columns in each subfigure are the axial views, and the next is the sagittal view.

segmented points from ultrasound images for this specific vertebra is less than all others (455 compared to average of 2466 for other vertebrae). Additionally, results for extremity vertebrae are worse. This can be explained by less constraint on their motion during registration.

Registrations in the region of interest, i.e., facet joints, have a mean TRE_f of 1.99 mm with a standard deviation of 1.0 mm and success rate of 87%.

For capture range experiment, 20 trials are performed, for each phantom and each interval, i.e., 100 trials for each interval including all phantoms. The results are depicted in Fig. 8. The success rate is above 95% for middle vertebrae (L2–L4) with initial TRE_b of less than 12 mm.

IV.C. Sheep cadaver registration

IV.C.1. Rigid registration

Rigid registration is performed on sheep cadaver data including five vertebrae (L1–L5). The UKF-based registration with outlier removal is performed 100 times. Registered vertebrae have a mean TRE_b of 2.73 mm with a standard deviation of 1.90 mm and success rate of 87%.

IV.C.2. Multibody rigid registration

Validation of the multibody registration technique was performed on the sheep cadaver data. An example of the registration results is shown in Fig. 9. The multibody registration is performed 100 times. We set variables α and n_g to be 0.1 and 2, respectively. Table IV shows the final error and success rate for each vertebra separately and for the average of them. Both TRE_b and TRE_f are computed here as well. We excluded the results where the algorithm did not converge. Registered vertebrae have a mean TRE_b of 3.1 mm with a standard deviation of 0.4 mm. Overall, 39% of vertebrae are registered with TRE_b of less than 3 mm. Registrations in the region of interest (facet joints) have a mean TRE_f of 2.2 mm with a standard deviation of 0.7 mm and success rate of 82%.

In comparison to phantom data, sheep cadaver yields larger final error for both rigid and multibody registrations.

TABLE III. TREs and percentage of success for group-wise registration for 100 registration trials on each phantom.

Patient	Error type	L1	L2	L3	L4	L5	Average	Success (%)
1	TRE_b	2.21 ± 0.7	2.08 ± 0.8	1.77 ± 0.5	1.50 ± 0.5	1.73 ± 1.5	1.86 ± 0.4	99
	TRE_f	1.79 ± 0.7	1.37 ± 0.8	1.27 ± 0.6	0.99 ± 0.4	1.62 ± 1.0	1.41 ± 0.3	100
2	TRE_b	3.03 ± 4.1	2.25 ± 2.2	2.62 ± 1.2	3.28 ± 0.8	4.94 ± 1.1	3.23 ± 2.4	66
	TRE_f	2.07 ± 2.3	1.78 ± 1.2	2.24 ± 1.5	3.07 ± 1.1	6.40 ± 1.1	3.11 ± 0.93	54
3	TRE_b	2.67 ± 1.9	2.31 ± 1.8	1.88 ± 1.3	1.73 ± 0.6	1.61 ± 0.5	2.04 ± 1.4	96
	TRE_f	2.31 ± 1.5	1.89 ± 1.5	1.35 ± 0.8	1.48 ± 0.5	1.36 ± 0.5	1.68 ± 0.7	98
4	TRE_b	3.27 ± 4.0	2.33 ± 1.4	1.88 ± 0.4	2.28 ± 0.5	2.83 ± 2.3	2.52 ± 2.2	90
	TRE_f	1.95 ± 1.6	1.58 ± 0.6	1.66 ± 0.6	2.13 ± 0.6	1.47 ± 1.5	1.76 ± 0.6	96
5	TRE_b	3.58 ± 4.5	2.90 ± 3.0	2.06 ± 0.8	2.37 ± 1.8	2.70 ± 2.3	2.72 ± 2.8	90
	TRE_f	2.29 ± 2.4	2.09 ± 1.1	1.81 ± 0.7	1.79 ± 1.1	2.06 ± 2.3	2.01 ± 1.0	90
All	TRE_b	2.95 ± 3.4	2.37 ± 2.0	2.04 ± 1.0	2.23 ± 1.1	2.76 ± 2.1	2.47 ± 1.4	
Percentage of $TRE_b < 3$	86	90	93	82	70	88		
All	TRE_f	2.08 ± 1.8	1.74 ± 1.1	1.67 ± 1.0	1.89 ± 1.1	2.58 ± 2.4	1.99 ± 1.0	
Percentage of $TRE_f < 3$	92	94	94	87	87	87		

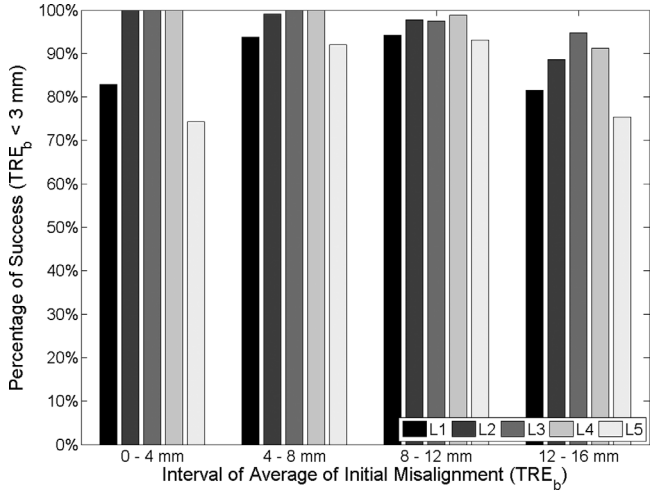

FIG. 8. The success rate (percentage of final TRE_b be less than 3 mm) is plotted for four intervals (from 0–4 to 12–14 mm) of average initial misalignment TRE_b. The success rate for three middle vertebrae (L2–L5) is maintained above 95% for up to 12 mm average of initial misalignment.

This result is expected, as the segmentation of the bone surface in ultrasound images is less accurate in real tissue. A large portion of the final TRE_b values in sheep cadaver are distributed between 3 and 5 mm, and almost all of the registrations have final TRE_b of less than 5 mm (success rate = 98%). Although the bounding box error shows higher error with respect to phantom data, the error around the region of interest, i.e., facet joints, is almost the same with comparable success rate with respect to phantom data (82% compared to 87%).

Similar to phantom data, capture range is computed for sheep cadaver with similar experiments. This time, the success rate is computed for the region of interest, i.e., facet joints. The result is depicted in Fig. 10. The success rate is above 95% for middle vertebrae (L2–L4) with initial TRE_b of less than 16 mm. This capture range is wide enough to cover any realistic initial misalignment expected to happen in operating room. Additionally, success rate is above 90% for the extremity vertebrae (L1 and L5) with initial TRE_b of less than 12 mm.

TABLE IV. TREs and percentage of success for group-wise registration for 100 registration trials on sheep cadaver.

	L1	L2	L3	L4	L5	All
TRE_b	3.5±1.1	2.7±0.8	2.8±0.3	2.7±0.8	3.9±1.2	3.1±0.4
$TRE_b < 3$ mm (%)	33	68	69	70	23	39
$TRE_b < 5$ mm (%)	87	98	100	98	87	98
TRE_f	2.3±0.9	1.8±0.6	2.1±0.4	2.2±0.5	2.6±0.7	2.2±0.7
$TRE_f < 3$ mm (%)	64	86	93	91	73	82

IV.D. Curved phantom registration

Validation of the multibody registration technique was performed on the curved phantom data. The multibody registration is performed 100 times. In each trial, a random initial rigid misalignment with parameters drawn randomly within ± 10 mm and $\pm 10^\circ$ is applied. We set variables α and n_g to be 0.1 and 2, respectively. The results can be found in Table V. The TRE is below 3.5 mm for all vertebrae, and all registrations have TRE below 5 mm.

Successful registration of the curved phantom data reveals the insensitivity of the algorithm to the physically realistic deformation of the spine curvature.

IV.E. Multibody rigid registration parameters

The results of multibody registration for different value of α are depicted in Fig. 11. This parameter affects the tradeoff between the point registration errors and the constraints imposed by the biomechanical model on the spine curvature. The worst results are achieved for $\alpha = 1$ where the biomechanical model is removed [see Eq. (4)]. When $\alpha = 10$, the cost function only contains the biomechanical model without considering the image alignment errors, and hence, the

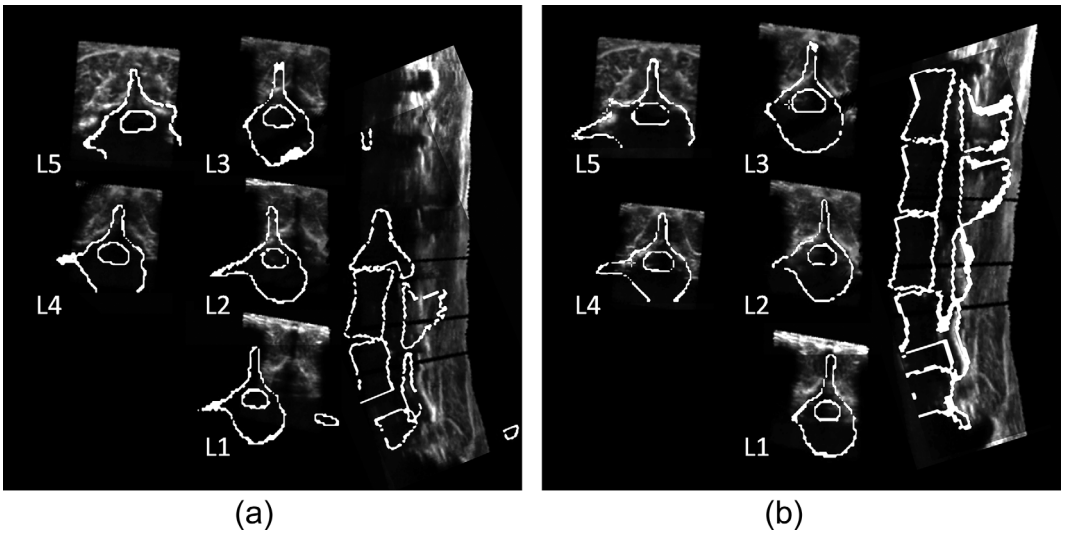

FIG. 9. An example of registration performed on sheep data. (a) The initial alignment of ultrasound and CT points and (b) the final alignment after registration. The first two columns in each subfigure are the axial views, and the next is the sagittal view.

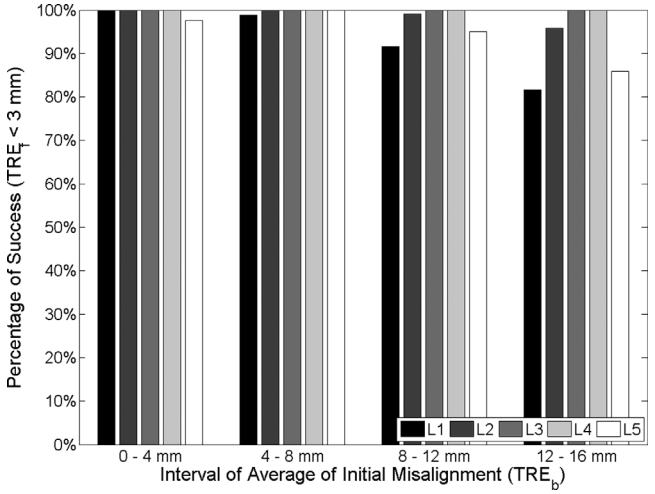

FIG. 10. The success rate (percentage of final TRE_f be less than 3 mm) is plotted for four intervals (from 0–4 to 12–14 mm) of average initial misalignment TRE_b. The success rate for three middle vertebrae (L2–L5) is maintained above 95% for up to 16 mm average of initial misalignment.

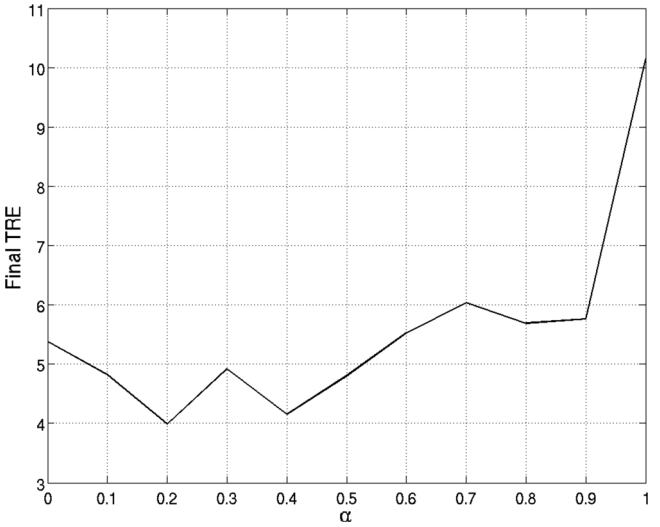

FIG. 11. Final TRE_b for different values of α. The transformation becomes a rigid one for all vertebrae together for $\alpha = 0$, whereas $\alpha = 1$ removes the biomechanical model, and therefore the motion of vertebrae is not constrained. Minimum error is achieved between these two values.

results are not relevant. Note that the terms E and G have different dynamic ranges. Selected value for α used in previous experiments ($\alpha = 0.1$) ensures that the contributions of E and G terms in Eq. (4) are similar. As such, the multibody registration cost function is different from the one for the rigid body registration alone.

The results of multibody registration for different number of grids (n_g) are shown in Table VI. Denser grid leads to a better simulation of the tissue connecting two adjacent vertebrae, but more registration runtime.

V. DISCUSSION

The presented work aims to improve the computational runtime of the registration by utilizing a feature-based approach. This technique requires ultrasound segmentation prior to performing any registration. However, by utilizing a fast ultrasound segmentation technique proposed by Foroughi *et al.*,[24] the runtime of this step is almost negligible. Since the current implementation of the registration algorithm in MATLAB is almost twice as fast as our previously proposed intensity-based approach,[8] we believe that proposed feature-based algorithm has higher potential for real-time applications, with parallel implementation. Clearly, the trade-off between time and accuracy has to be considered.

The algorithm parameters are learned from the phantom data with normal curvature only and are used in both the curved phantom data and the sheep cadaver. The result of registration on the sheep cadaver data shows the effectiveness of the approach across different data sets, possibly with nonoptimum parameters. To further investigate the effect of the parameters, we performed registration with different values of n_g and α. The results are presented in Table VI and Fig. 11. Changing the algorithm parameters may have effects on the result. The results become worse as α changes toward 0 or 1, meaning that both parts of the cost function defined in Eq. (4) are essential for a successful registration. Additionally, denser grid (higher n_g) leads to better result but more computation time.

In the current framework, preoperative CT segmentation, initialization of the CT-derived model location within the ultrasound volume, and the algorithm parameters (i.e., n_g and α) should be performed manually. Preoperative CT can be segmented prior to the intervention and does not add to the computation time. However, its low accuracy may affect the CT to ultrasound registration result. We showed that the registration result is not sensitive to any realistic initial misalignment. We also demonstrated that manual selection of the algorithm parameters may affect the result. However, the results stay the same for a relatively large range of selections

TABLE V. TREs for group-wise registration for 100 registration trials of the curved phantom.

	L2	L3	L4	All
Natural to curved	3.7 ± 1.4	3.8 ± 0.3	2.8 ± 0.4	3.5 ± 1.0
TRE < 3 mm (%)	39	0	68	7
TRE < 5 mm (%)	86	100	100	100
Curved to natural	3.8 ± 1.4	2.7 ± 0.5	3.2 ± 0.6	3.2 ± 1.0
TRE < 3 mm (%)	21	85	35	42
TRE < 5 mm (%)	85	100	100	100

TABLE VI. Final TRE_b for registration using different number of springs. The registration becomes more accurate with higher number of springs but take more time to run.

n_g	Final TRE_b (mm)	Time (min)
1	10.93	8
2	3.78	30
3	3.18	37
4	3.16	85

($0.1 \leq \alpha \leq 0.5$ and $n_g \geq 2$), meaning that the optimum parameters can be easily identified.

The only similar work to what is presented in our paper is performed by our group[8] which is evaluated using the same data set as we use here. In Gill *et al.*,[8] following an intensity-based approach implemented in C++, CT images of three vertebrae are registered (L2–L4) to ultrasound images. The runtime for that algorithm is around 40 min. On the other hand, registration and segmentations presented in our work are implemented in MATLAB that is typically an order of magnitude slower than a C++ implementation. The segmentation for all ultrasound images together (around 250 2D US images) takes less than a minute. The registration runtime including the ultrasound segmentation is 20 min for registration performed on the phantom data and 29 min for registration performed on the sheep cadaver, and 15 min for the naturally curved phantom. Note that the phantom data and the sheep cadaver contain five vertebrae, whereas the naturally curved phantom contains only three vertebrae. Given that, in the same scenario (including three vertebrae in the registration), our algorithm is computationally substantially less expensive, compared to the intensity-based registration performed by Gill *et al.*[8] (compare 15 min in a MATLAN implementation to 40 min in C++). It should be noted that our achieved mean registration error (TRE_b of 2.47 mm) is slightly worse than that achieved by the intensity-based registration technique of Gill *et al.* (TRE_b is 1.97 mm); however, both algorithms produce registration errors that are within the clinically acceptable ranges for spinal anesthesia procedures.[8] On the other hand, intensity-based approach has a wider capture range and less failure rate, which suggests that the feature-based method proposed here requires more accurate initial manual alignment between the CT and US data for successful registration.

VI. CONCLUSION

This paper presented a biomechanically constrained multibody rigid registration algorithm for aligning intraprocedure ultrasound and preprocedure CT images of the lumbar spine. Multibody registration is performed as the patient has different posture between preoperative image acquisition and intervention which leads to a difference in the spine curvature between CT and ultrasound images. Individual transformation parameters are considered for each vertebra.

We developed a biomechanical model to constrain the multibody UKF-based registration algorithm and have integrated the registration framework with a fast 2D ultrasound segmentation approach.

We showed the validation of the algorithm on human phantom data and a sheep cadaver. All registrations began with an initial misalignment between 0 and 20 mm. For the patient-based phantoms, the final TRE_b had an average of 2.47 mm, and 88% of the multibody registration achieved a clinically acceptable registration ($TRE_b < 3$ mm). For the sheep cadaver data, the final TRE_b had an average of 3.1 mm and 98% of multibody registrations had TRE_b less than 5 mm. The results for human phantom data show higher success than the sheep cadaver. This can be because of the lower accuracy of ultrasound segmentation in the real tissues. However, the registration accuracy is almost the same around the region of interest, i.e., facet joints. For the patient-based phantoms, the final TRE_f had an average of 1.99 mm, and 87% of multibody registrations had TRE_f less than 3 mm. For the sheep cadaver data, the final TRE_f had an average of 2.2 mm, and 82% of multibody registrations had TRE_f less than 3 mm.

The multibody rigid registration has the potential of parallel implementation. Future work will mainly focus on decreasing the runtime and techniques for more accurate segmentation of ultrasound images. Additionally, the registration will be integrated into a graphical user interface to be used for guiding the anesthesia injections.

ACKNOWLEDGMENTS

This research is funded by the Canadian Institutes of Health Research (CIHR) and the Natural Sciences and Engineering Research Council (NSERC) of Canada. The authors gratefully acknowledge the assistance of Dr. Mehdi Hedjazi Moghari, Pezhman Foroughi and Sean Gill in this research.

[a]Author to whom correspondence should be addressed. Electronic mail: purang@ece.ubc.ca

[1]M. Mahowald, J. Singh, and P. Majeski, "Opioid use by patients in an orthopedics spine clinic," Arthritis Rheum. **52**(1), 312–321 (2005).
[2]M. Pathria, D. Sartoris, and D. Resnick, "Osteoarthritis of the facet joints: Accuracy of oblique radiographic assessment," Radiology **164**(1), 227–230 (1987).
[3]T. Laine, T. Lund, M. Ylikoski, J. Lohikoski, and D. Schlenzka, "Accuracy of pedicle screw insertion with and without computer assistance: A randomised controlled clinical study in 100 consecutive patients," Eur. Spine J. **9**(3), 235–240 (2000).
[4]R. Klocke, T. Jenkinson, and D. Glew, "Sonographically guided caudal epidural steroid injections," J. Ultrasound Med. **22**(11), 1229–1232 (2003).
[5]K. Galiano, A. A. Obwegeser, C. Walch, R. Schatzer, F. Ploner, and H. Gruber, "Ultrasound-guided versus computed tomography-controlled facet joint injections in the lumbar spine: A prospective randomized clinical trial," Reg. Anesth. Pain Med. **32**(4), 317–322 (2007).
[6]B. Brendel, J. Siepermann, S. Winter, and H. Ermert, "*In vivo* evaluation and *in vitro* accuracy measurements for an ultrasound-CT registration algorithm," Comput. Assist. Radiol. Surg. **1281**(1), 583–588 (2005).
[7]E. C. S. Chen, P. Mousavi, S. Gill, G. Fichtinger, and P. Abolmaesumi, "Ultrasound guided spine needle insertion," Proc. SPIE **7625**, 762538 (2010).
[8]S. Gill, P. Abolmaesumi, G. Fichtinger, J. Boisvert, D. Pichora, D. Borshneck, and P. Mousavi, "Biomechanically constrained groupwise ultrasound to CT registration of the lumbar spine," Med. Image Anal. **16**(3), 662–674 (2012).
[9]J. Moore, C. Clarke, D. Bainbridge, C. Wedlake, A. Wiles, D. Pace, and T. Peters, "Image guidance for spinal facet injections using tracked ultrasound," in *Medical Image Computing and Computer-Assisted Intervention* (Springer Berlin/Heidelberg, London, UK, 2009), pp. 516–523.
[10]D. M. Muratore, B. M. Dawant, and J. Robert L. Galloway, "Vertebral surface extraction from ultrasound images for technology-guided therapy," Proc. SPIE **3661**, 1499–1510(1999).
[11]H. Talib, M. Peterhans, J. Garca, M. Styner, and M. Gonzlez Ballester, "Kalman filtering for frame-by-frame CT to ultrasound rigid registration," in *Medical Imaging and Augmented Reality* (Springer Berlin/Heidelberg, Tokyo, Japan, 2008), Vol. 5128, pp. 185–192.
[12]S. Winter, B. Brendel, I. Pechlivanis, K. Schmieder, and C. Igel, "Registration of CT and intraoperative 3D ultrasound images of the spine using evolutionary and gradient-based methods," IEEE Trans. Evol. Comput. **12**(3), 284–296 (2008).

[13]D. Amin, T. Kanade, A. M. D. Gioia, and B. Jaramaz, "Ultrasound registration of the bone surface for surgical navigation," Comput. Aided Surg. **8**(1), 1–16 (2003).
[14]C. S. K. Chan, P. J. Edwards, and D. J. Hawkes, "Integration of ultrasound-based registration with statistical shape models for computer-assisted orthopaedic surgery," Proc. SPIE **5032**, 414–424 (2003).
[15]D. Barratt, P. Penney, S. Chan, M. Slomczykowski, T. Carter, P. Edwards, and D. Hawkes, "Self-calibrating 3D-ultrasound-based bone registration for minimally invasive orthopedic surgery," IEEE Trans. Med. Imaging **25**(3), 312–323 (2006).
[16]B. Brendel, S. Winter, A. Rick, M. Stockheim, and H. Ermert, "Registration of 3D CT and ultrasound datasets of the spine using bone structures," Comput. Aided Surg. **7**(3), 146–155 (2002).
[17]H. Talib, M. Styner, T. Rudolph, and M. A. Gonzalez Ballester, "Dynamic registration using ultrasound for anatomical referencing," in *IEEE International Symposium on Biomedical Imaging: From Nano to Macro—ISBI* (IEEE, Arlington, VA, 2007), pp. 1164–1167.
[18]M. Peterhans, H. Talib, M. G. Linguraru, M. Styner, and M. A. G. Ballester, "A method for frame-by-frame US to CT registration in a joint calibration and registration framework," in *IEEE International Symposium on Biomedical Imaging: From Nano to Macro—ISBI* (IEEE, Arlington, VA, 2008), pp. 1131–1134.
[19]S. Winter, I. Pechlivanis, C. Dekomien, C. Igel, and K. Schmieder, "Toward registration of 3D ultrasound and CT images of the spine in clinical praxis: Design and evaluation of a data acquisition protocol," Ultrasound Med. Biol. **35**(11), 1773–1782 (2009).
[20]J. Salvia, C. Mataboscha, D. Fofib, and J. Foresta, "A review of recent range image registration methods with accuracy evaluation," Image Vis. Comput. **25**(5), 578–596 (2007).
[21]M. H. Moghari and P. Abolmaesumi, "Point-based rigid-body registration using an unscented Kalman filter," IEEE Trans. Med. Imaging **26**(12), 1708–1728 (2007).
[22]M. H. Moghari and P. Abolmaesumi, "Global registration of multiple bone fragments using statistical atlas models: Feasibility experiments," in *IEEE Engineering in Medicine and Biology Society—EMBS*, pp. 5374–5377 (IEEE, Vancouver, Canada, 2008).
[23]P. Besl and H. McKay, "A method for registration of 3-D shapes," IEEE Trans. Pattern Anal. Mach. Intell. **14**(2), 239–256 (1992).
[24]P. Foroughi, E. Boctor, M. J. Swartz, R. H. Taylor, and G. Fichtinger, "Ultrasound bone segmentation using dynamic programming," in *IEEE Ultrasonics Symposium* (IEEE, New York, 2007), pp. 2523–2526.
[25]R. Czerwinski, D. Jones, and J. O'Brien, W. D., "Line and boundary detection in speckle images," IEEE Trans. Image Process **7**(12), 1700–1714 (1998).
[26]P. Abolmaesumi and M. R. Sirouspour, "Segmentation of prostate contours from ultrasound images," in *IEEE International Conference on Acoustics, Speech, and Signal Processing* (IEEE, Montreal, Quebec, Canada, 2004), Vol. 3, pp. 517–520.
[27]T. K. Chen, A. D. Thurston, R. E. Ellis, and P. Abolmaesumi, "A real-time freehand ultrasound calibration system with automatic accuracy feedback and control," Ultrasound Med. Biol. **35**(1), 79–93 (2009).
[28]T. K. Chen, R. E. Ellis, and P. Abolmaesumi, "Improvement of freehand ultrasound calibration accuracy using the elevation beam width profile," Ultrasound Med. Biol. **37**(8), 1314–1326 (2011).
[29]S. H. Zhou, I. D. McCarthy, A. H. McGregor, R. R. H. Coombs, and S. P. F. Hughes, "Geometrical dimensions of the lower lumbar vertebrae analysis of data from digitized CT images," Eur. Spine J. **9**(3), 242–248 (2000).
[30]W. Wein, B. Roper, and N. Navab, "Automatic registration and fusion of ultrasound with CT for radiotherapy," in *Medical Image Computing and Computer-Assisted Intervention* (Springer Berlin/Heidelberg, Palm Springs, CA, 2005), pp. 303–311.
[31]B. K. P. Horn, "Closed-form solution of absolute orientation using unit quaternions," J. Opt. Soc. Am. **5**(7), 1127–1135 (1987).
[32]M. Greher, L. Kirchmair, B. Enna, P. Kovacs, B. Gustorff, S. Kapral, and B. Moriggl, "Ultrasound-guided lumbar facet nerve block: Accuracy of a new technique confirmed by computed tomography," Anesthesiology **101**(5), 1195–1200 (2004).
[33]M. M. Panjabi, T. Oxland, K. Takata, V. Goel, J. Duranceau, and M. Krag, "Articular facets of the human spine. quantitative three-dimensional anatomy," Spine **18**(10), 1298–1310 (1993).